Detection of terahertz radiation in gated two-dimensional structures governed by dc current

D. Veksler,[1] F. Teppe,[1,2] A. P. Dmitriev,[1,2,3] V. Yu. Kachorovskii,[1,2,3] W. Knap,[1,2] and M. S. Shur[1]
[1]*Rensselaer Polytechnic Institute, 110, 8th Street, Troy, New York 12180, USA*
[2]*GES CNRS-Universite Montpellier 2, UMR 5650, 34900 Montpellier, France*
[3]*A.F. Ioffe Physical-Technical Institute, 26 Polytechnicheskaya Street, Saint Petersburg, 194021, Russia*
(Received 24 May 2005; revised manuscript received 23 December 2005; published 21 March 2006)

We present theoretical and experimental studies of the direct current effect on the detection of subterahertz and terahertz radiation in gated two-dimensional structures. We developed a theory of the current-driven detection both for resonant case, when the fundamental frequency of plasma oscillation is large compared to inverse scattering time, $\omega_0\tau \gg 1$, and for the nonresonant case, $\omega_0\tau \ll 1$, when the plasma oscillations are damped. We predict that, in the nonresonant case, even a very small dc current would increase the detection amplitude up to two orders of magnitude. Physically, this increase is related to an abrupt transition from the linear to saturation region near the knee of the current-voltage characteristic. When the current increases up to the saturation value, the electron concentration near the drain becomes very low and can be strongly affected by a small external field. As a consequence, the two-dimensional channel becomes extremely sensitive to external perturbations. In the resonant case, the detection amplitude has maxima when the radiation frequency is equal to fundamental plasma frequency and its harmonics. We predict that the effective linewidths of the respective resonances would decrease with the increasing current. Physically, this happens because dc current shifts the system towards the plasma wave instability. At some critical current value, the width corresponding to the fundamental frequency would turn to zero, indicating the onset of plasma waves generation. Our experimental measurements performed on GaAs HEMT confirm the theoretical predictions.

DOI: 10.1103/PhysRevB.73.125328 PACS number(s): 73.21.−b, 73.22.−f, 73.23.Ad, 73.50.Fq

I. INTRODUCTION

Plasma waves in a gated two-dimensional (2D) structure have a linear dispersion law $\omega(k)=sk$,[1] where s is the wave velocity. A structure of a given length, L, acts for these waves as a resonant "cavity," having a quality factor of the order of $s\tau/L$, where τ is the momentum relaxation time. The simplest realization of such structure is the channel of the field effect transistor (FET). The dramatic reduction of device sizes in the last decades has led to the development of new generations of FETs, which may have high quality factors. Such FETs should demonstrate novel physics, specific for ballistic regime.[2] In particular, at certain boundary conditions, the stationary current flow in such a FET should become unstable with respect to formation the resonant plasma oscillations with the frequencies[3]

$$\omega_N = \omega_0(1+2N), \tag{1}$$

where $\omega_0=\pi s/2L$, and $N=0,1,2,\ldots$. Due to the coupling with electromagnetic waves, the instability should lead to generation of radiation with the same frequencies.

The plasma wave velocity $s=\sqrt{e^2n/mC}$ depends on the carrier density in the channel n and the gate to channel capacitance per unit area $C=\epsilon/4\pi d$, where e is the electron charge, m is the electron effective mass, d is the gate-to-channel distance, and ϵ is the dielectric constant. In the gradual channel approximation

$$n = \frac{CU_g}{e}, \tag{2}$$

where $U_g=V_{gs}-V_{th}$ is the difference between the gate-to-source voltage V_{gs} and the threshold voltage V_{th}. Hence, plasma wave velocity is controlled by gate voltage

$$s = \sqrt{\frac{eU_g}{m}}. \tag{3}$$

In a short channel FET, the oscillation frequency, $\omega_0/2\pi$, may be tuned by gate voltage to be in terahertz range. As a consequence, the plasma wave instability should lead to generation of terahertz radiation,[3] thus promising to close the famous "terahertz gap," moving from the low frequency electronic side.

The instability may take place both in the hydrodynamic regime[3] (fast electron-electron collisions) and in the collisionless plasma regime.[4] In the former case, the dynamics of plasma waves is described by equations which coincide with the hydrodynamic equations for shallow water[3] [see Eqs. (4) and (5) below]. The hydrodynamic analogy has profound consequences for understanding of physics of 2D electrons in the ballistic FET. Phenomena similar to nonlinear waves propagation,[5] hydraulic jump,[6] and the "choking" effect[7] should take place in the electron fluid. Based on this analogy, a variety of possible applications of FET operating as a THz device have been suggested.[3,8] In particular, it was shown that the nonlinear properties of plasma oscillations can be utilized for terahertz detectors, broadband detectors, mixers, and frequency multipliers.[9] Note also that the nonlinear hydrodynamic effects limit the development of the plasma wave instability,[5] yielding a square-root dependence of developed plasma oscillations on the dc current above the instability threshold.

The experimental exploration of the subject began a long time ago, starting from the observation of infrared

 ©2006 The American Physical Society

absorption[10] and weak infrared emission[11] related to plasma waves in silicon inversion layers. Later, the nonresonant detection[12,13] and weak resonant detection[14] were observed in high mobility transistors. It was also shown that the impedance of a high mobility transistor exhibits maxima at the fundamental plasma frequency and its harmonics.[15] Recently, interest in the study of plasma waves in ballistic FETs increased dramatically. A new boost to the research in this direction was given by a series of publications[16–24] reporting observation of the terahertz detection and emission in ballistic high electron mobility transistors (HEMTs) fabricated from different materials. The publication reporting nonresonant terahertz detection in GaAs-based commercial HEMT[16] was followed by several others demonstrating resonant terahertz detection in GaAs-based commercial HEMTs,[17,18] in Si metal-oxide-semiconductor field effect transistor (MOSFET),[19] nitride based HEMTs,[20] and in gated double quantum well heterostructures.[21,22] In all devices, the 2D plasmon was tuned to the frequency of terahertz radiation by varying the gate bias. The most remarkable results have been reported in the past several months: the plasma waves emission was demonstrated in an InGaAs-based HEMT gate[23] and in GaN-based HEMT,[24] and room temperature resonant detection was reported in InGaP/InGaAs/GaAs HEMT[25] and in GaAs/AlGaAs HEMT.[26]

The experiments on nonresonant and resonant detection seem to be in a good agreement with the theory.[9] As for emission measurements, the situation is more subtle. The reported THz emission[23,24] had a threshold character as had been predicted in Ref. 3. The resonant frequency value and the range of its shift by the gate-to-source bias were in a reasonable agreement with the theory. However, the emission was observed close to the velocity saturation regime or even deeply in the saturation regime. Therefore, the effects specific for hot electron physics might play an important role. Such effects are known to lead to different instabilities caused by electron "runaway" phenomenon.[27,28] In particular, transit time effects,[29,30] enhanced emission of optical phonons,[31] and stratification of electron flow[32] might lead to the plasma wave excitation. In contrast to this, the mechanism proposed in Ref. 3 relates terahertz generation to the amplification of plasma waves on the boundaries of the channel and might take place in the ohmic regime when electrons are "cold." To understand the underlying physics of the observed emission, additional experiments and theoretical investigations should be carried out. In this aspect, the study of the source-to-drain dc current effect on the THz detection looks very promising. It is this current that might lead to the plasma wave instability,[3] thus turning the system from the detection to the generation regime.

In this paper, we study theoretically the effect of source-to-drain dc current on the detection of the terahertz radiation both in resonant and nonresonant regime. We also present experimental study of THz detection governed by source-to-drain dc current for nonresonant case. A theory of detection at zero current was developed in Ref. 9. It was shown that a FET, biased by the gate-to-source voltage and subjected to electromagnetic radiation with frequency ω, can develop a constant drain-to-source voltage δU^*, which at $\omega_0\tau \gg 1$ has a resonant dependence on the radiation frequency ω with the maxima at ω_N. Here we demonstrate (both experimentally and theoretically) that the detection is drastically modified by dc current. We show that source-to-drain current I_d leads to a very sharp increase of the detection efficiency by a factor of two orders compared to the zero current case. A similar result was observed before.[33] It was reported that the detection sharply increases with increasing I_d. This increase was attributed to a sharp decrease of the gate-to-drain capacitance. In this paper, we present a detailed theoretical description of the phenomenon and derive the analytical expression for the detector response both in resonant and nonresonant cases. The results we obtain for the nonresonant case support the qualitative explanation presented in Ref. 33. These results also allow us to explain our experiments. For the resonant case, we predict the decreasing of the resonance width with increasing the current. As expected, at some critical value of the current, the width becomes zero, which implies the onset of the plasma wave instability.

II. BASIC EQUATIONS

In this section, we will modify the previously developed theory[9] to include a dc current. We assume that electron-electron collisions are very fast, turning the system into the hydrodynamics regime. The hydrodynamic equations, describing a two-dimensional electronic fluid in FET channel, are the equation of motion (the Euler equation) and the usual continuity equation

$$\frac{\partial v}{\partial t} + v\frac{\partial v}{\partial x} + \frac{v}{\tau} = -\frac{e}{m}\frac{\partial U}{\partial x}, \tag{4}$$

$$\frac{\partial U}{\partial t} + \frac{\partial (Uv)}{\partial x} = 0, \tag{5}$$

where U is the local value of the gate-to-channel voltage, $\partial U/\partial x$ is the longitudinal electric field in the channel, v is the local electron velocity, and e is the absolute value of the electron charge. Equation (5) takes into account that, in the gradual channel approximation, the local density in the electron channel is related to the local value of the gate-to-channel voltage as

$$n = \frac{CU}{e}, \tag{6}$$

which is a simple generalization of Eq. (2). Equations (4) and (5) require two boundary conditions, which depend on the properties of contacts. Following Ref. 3, we assume that the voltage is fixed at the left side of the channel and the current flowing through the right side of the channel does not depend on time and is equal to I_d,

$$U(0) = U_g + U_a \cos \omega t, \tag{7}$$

$$U(L)v(L) = \frac{j_d}{C}. \tag{8}$$

Here $j_d = |I_d|/W$ is the absolute value of the current density (since the electron moves from source to drain, the current is

negative), and W is the channel width. In Eq. (7) we assumed that radiation leads to the gate-voltage oscillations with the amplitude U_a and the frequency ω. The basic idea of detection is that such oscillations induce a constant source-to-drain voltage[9]

$$\delta U^* \sim U_a^2 \tag{9}$$

In the next sections we will show that the coefficient proportionality between δU^* and U_a^2 increases sharply with increasing I_d.

III. NONRESONANT DETECTION

In the nonresonant case, $\omega_0 \tau \ll 1$ and $\omega \tau \ll 1$. The condition $\omega\tau \ll 1$ allows us to neglect the $\partial v/\partial t$ term in Eq. (4). We will neglect also the term $v\partial v/\partial x$. The corresponding criterion will be presented below. Thus, Eq. (4) simplifies

$$\frac{e}{m}\frac{\partial U}{\partial x} + \frac{v}{\tau} = 0. \tag{10}$$

Substituting Eq. (10) into Eq. (5) we get

$$\frac{\partial U}{\partial t} = \frac{\mu}{2}\frac{\partial^2 U^2}{\partial x^2}, \tag{11}$$

where $\mu = e\tau/m$ is the electron mobility. The boundary conditions for Eq. (11) follow from Eqs. (7), (8), and (10),

$$U(0) = U_g + U_a \cos \omega t, \tag{12}$$

$$\left(\frac{\partial U^2}{\partial x}\right)_{x=L} = -\frac{2j_d}{\mu C}. \tag{13}$$

In absence of radiation ($U_a=0$) we obtain from Eqs. (11)–(13) the stationary voltage-current characteristic

$$j_d = \frac{\mu C}{L}\left(U_g U^* - \frac{U^{*2}}{2}\right), \tag{14}$$

where $U^* = U_g - U(L)$ is the voltage drop across the channel. This expression is valid for $U^* \leqslant U_g$. At $U^* = U_g$, the electron concentration at the drain turns to zero $[n(L) = CU(L)/e = 0]$ and current reaches the value

$$j_{sat} = \frac{\mu C U_g^2}{2L}. \tag{15}$$

Physically, j_{sat} is the saturation current in the Shockley model which neglects velocity saturation[34] [actually, at some value of current smaller than j_{sat}, but very close to j_{sat}, velocity saturates and Eq. (14) becomes invalid]. In this paper, we restrict ourselves to the case $U^* < U_g$ and, respectively, $j_d < j_{sat}$, neglecting velocity saturation effect.

For $U_a \neq 0$, we search the solution of Eq. (11) in the form

$$U = U_0(x) + \frac{1}{2}U_1 e^{-i\omega t} + \frac{1}{2}U_1^* e^{i\omega t}. \tag{16}$$

We neglected here the contribution of higher harmonics. The corresponding criterion will be given below. First, we separate oscillating and stationary terms in Eqs. (11) and (13). The stationary term obeys

$$\frac{\partial^2}{\partial x^2}\left(U_0^2 + \frac{1}{2}|U_1|^2\right) = 0, \tag{17}$$

with the boundary conditions

$$U_0(0) = U_g; \quad \left[\frac{\partial}{\partial x}\left(U_0^2 + \frac{1}{2}|U_1|^2\right)\right]_{x=L} = -\frac{2j_d}{\mu C}. \tag{18}$$

The spatial dependence of oscillating amplitude U_1 is described by the following equation:

$$-\frac{i\omega}{\mu}U_1 = \frac{\partial^2 (U_1 U_0)}{\partial x^2}. \tag{19}$$

The boundary conditions for this equation are

$$U_1(0) = U_a, \quad \left[\frac{\partial (U_1 U_0)}{\partial x}\right]_{x=L} = 0. \tag{20}$$

The solution of Eq. (17) with boundary conditions (18) is given by

$$U_0^2(x) + \frac{|U_1(x)|^2}{2} = U_g^2 + \frac{U_a^2}{2} - \frac{2j_d}{\mu C}x. \tag{21}$$

The quantity U_1 is proportional to small amplitude U_a. Thus in zero approximation we can neglect $|U_1|^2$ (as well as U_a^2) in Eq. (21). As a result we have

$$U_0(x) = U_g\sqrt{1 - \lambda x/L}, \tag{22}$$

where

$$\lambda = \frac{j_d}{j_{sat}}. \tag{23}$$

Using Eqs. (6) and (22) we find stationary electron distribution in the channel

$$n_0(x) = \frac{CU_g}{e}\sqrt{1 - \lambda x/L}. \tag{24}$$

As follows from Eqs. (22) and (24), in the absence of radiation, the potential and concentration at the drain are given by

$$U_0(L)|_{U_a=0} = U_g\sqrt{1-\lambda}, \quad n_0(L)|_{U_a=0} = \frac{CU_g}{e}\sqrt{1-\lambda}. \tag{25}$$

Since $U^* = U_g - U_0(L)$, radiation induced change of the source-to-drain voltage is given by $\delta U^* = -\delta U_0(L)$, where $\delta U_0(L) = U_0(L) - U_0(L)|_{U_a=0}$. To avoid any confusion in signs, in what follows we will call $\delta U_0(L)$ the detector response. From Eqs. (21) and (25) we find

$$\delta U_0(L) \approx \frac{U_a^2 - |U_1(L)|^2}{4U_g\sqrt{1-\lambda}}. \tag{26}$$

Therefore, to find response, we need to calculate $U_1(L)$. Introducing the function

$$f = \frac{U_1 U_0}{U_a U_g} \tag{27}$$

and substituting Eq. (22) into Eq. (19), we get

$$\frac{d^2 f}{dy^2} = -i \frac{\epsilon_0}{\sqrt{1-\lambda y}} f. \tag{28}$$

This equation should be solved with the boundary conditions

$$f(0) = 1, \quad f'(1) = 0. \tag{29}$$

Here $y = x/L$ and

$$\epsilon_0 = \frac{\omega L^2}{\mu U_g} = \frac{\pi^2}{4} \frac{\omega}{\omega_0^2 \tau} = \frac{L^2}{L_0^2}, \tag{30}$$

where $L_0 = s\sqrt{\tau/\omega}$. Physically, L_0 determines a characteristic spatial scale of the decay of the alternating component of voltage, U_1,[9] along the channel. Thus, for $\epsilon_0 \gg 1$, the oscillations excited at the source do not reach the drain.

First, we briefly recall the case of zero current (for a detailed discussion, see Ref. 9). In this case, $\lambda = 0$, and Eq. (28) is easily solved, yielding

$$U_1(L) = \frac{U_a}{\cosh(\sqrt{-i}L/L_0)}. \tag{31}$$

Equation (21) for zero current becomes

$$U_0(L) = \sqrt{U_g^2 + \frac{U_a^2 - |U_1(L)|^2}{2}} \approx U_g + \frac{U_a^2 - |U_1(L)|^2}{4U_g}. \tag{32}$$

In this equation we only kept the linear term with respect to U_a^2. It is worth noting that the precision of our calculations does not allow to account for higher order terms because we neglected high order harmonics in Eq. (16). For $L \gg L_0$, the oscillations on the drain are damped and $U_1(L) \to 0$. Hence, the response is given by[9]

$$\delta U_0(L) = \sqrt{U_g^2 + \frac{U_a^2}{2}} - U_g \approx \frac{U_a^2}{4U_g}. \tag{33}$$

In the opposite case, $L \ll L_0$, the oscillation amplitude on the drain is close to its value on the source $U_1(L) \approx U_a^2(1 - L^4/6L_0^4)$ and the response is given by[9]

$$\delta U_0(L) = \sqrt{U_g^2 + \frac{U_a^2}{12}\frac{L^4}{L_0^4}} - U_g \approx \frac{U_a^2}{24U_g}\frac{L^4}{L_0^4}. \tag{34}$$

We see that, in both cases, the response has the same sign, corresponding to the negative induced drain-to-source voltage. This sign is the consequence of a larger induced potential at the source side of the channel compared to drain side of the channel, where the ac potential is smaller, resulting in a smaller dc drain potential. Equations (33) and (34) predict the infinite growth of the response when $U_g \to 0$. We notice, however, that these equations are only valid if $U_g \gg U_a$. For $U_g \sim U_a$ one should take into account higher order harmonics in expansion Eq. (16).

Next we will calculate response for a nonzero current. The further consideration depends on the relation between L and L_0. We will see that, in contrast to the case $j_d = 0$, the response might change sign in short samples, when $L \ll L_0$.

A. Short samples

Consider first the case of short samples ($L \ll L_0$). As seen from Eq. (30) this is equivalent to the low frequency case ($\epsilon_0 = \omega\tau/\tau^2\omega_0^2 \ll 1$). Since $\epsilon_0 \ll 1$, we can search the solution of Eqs. (28) and (29) in series over the small parameter ϵ_0,

$$f(y) = 1 + i\epsilon_0 f_1(y) + \epsilon_0^2 f_2(y) + \cdots. \tag{35}$$

Substituting this expansion into Eq. (28) and having in mind Eqs. (21), (22), and (27) we get after some algebra

$$\delta U_0(L) = \frac{U_a^2}{4U_g(1-\lambda)^{3/2}}\left(-\lambda + \frac{4\epsilon_0^2}{15}\frac{5 + 4\sqrt{1-\lambda} + 1 - \lambda}{(1+\sqrt{1-\lambda})^4}\right). \tag{36}$$

Here we kept the terms which are proportional to U_a^2 only. We also neglected terms of the higher order of ϵ_0^3 and higher. For $\lambda \ll 1$, Eq. (36) simplifies

$$\delta U_0(L) \approx \frac{U_a^2}{4U_g}\left(-\lambda + \frac{\epsilon_0^2}{6}\right). \tag{37}$$

As seen, the response changes sign at relatively small currents $\lambda = \epsilon_0^2/6$. The second term in Eq. (37) is positive and represents the zero current response [see Eq. (34)].

To understand the physical meaning of the negative contribution, we note that the first term in the brackets in the r.h.s. of Eqs. (36) and (37) does not depend on radiation frequency. Consider the limiting case $\omega \to 0$ (i.e., $\epsilon_0 \to 0$). In this case, the instant value of the voltage at the drain can be found using stationary current-voltage characteristic of the channel given by Eq. (14). Expressing from Eq. (14) the voltage at the drain as a function of j_d and U_g we find $U(L) = \sqrt{U_g^2 - 2Lj_d/\mu C}$. In the case of very low frequencies this equation still holds with the replacement $U_g \to U_g + U_a\cos(\omega t)$. In other words, $U(L,t)$ adiabatically follows the instant value of the gate voltage,

$$U(L,t) = \sqrt{[U_g + U_a\cos(\omega t)]^2 - \frac{2Lj_d}{\mu C}}. \tag{38}$$

The stationary value of the voltage at the drain is found by averaging Eq. (38) over time, $U_0(L) = \langle U(L,t)\rangle$, and expanding the result up to the first order in U_a^2,

$$\delta U_0(L) = -\frac{\lambda}{(1-\lambda)^{3/2}}\frac{U_a^2}{4U_g}. \tag{39}$$

As seen, this equation coincides with the first term of Eq. (36). This reveals the physical meaning of change in sign, which is due to competition of two detection mechanisms: one is due to the damped plasma waves [with the response given by Eq. (34) or the second term in Eq. (37), which coincide], and the second is due to the current-induced asymmetry of the field distribution. The second mechanism is dominant when $\lambda \to 0$, i.e., at the saturation voltage, where the transistor is extremely sensitive to external perturbations (see discussion in Sec. VI).

B. Long samples

In this case $L \gg L_0$ (which is equivalent to demanding $\tau^2\omega_0^2 \ll \omega\tau \ll 1$). Since $\epsilon_0 \gg 1$ we can search for solution of Eq. (28) using the Wentzel-Kramers-Brillouin (WKB) approximation. In this approximation we obtain two solutions, one of them increases exponentially and another one decreases exponentially. The boundary condition (29) allows us to keep only the exponentially decreasing solution. This implies that $U_1(L) \to 0$ (with exponential precision). Thus, from Eq. (26) we find

$$\delta U_0(L) = \frac{U_a^2}{4U_g}\frac{1}{\sqrt{1-\lambda}}. \quad (40)$$

We see that in both cases, $L \gg L_0$ and $L \ll L_0$, the response sharply increases when $\lambda = j_d/j_{sat} \to 1$. This increase is caused by the increase in the nonuniformity of the potential and field distribution in the channel that increases the nonlinear properties of the FET (see discussion in Sec. VI).

To conclude this section we note that the theory of nonresonant detection developed above should be also valid for collisionless plasma, though we used hydrodynamic equations as a starting point. Indeed, in our calculations we neglected the "hydrodynamic" term $v\partial v/\partial x$ in Eq. (4). In other words, Eqs. (5) and (10) equally apply for cases when electron-electron collisions are absent or for dense plasma, where such collisions dominate. In the case of a dense plasma, the approximation, in which the hydrodynamic term is neglected becomes invalid both in long and short samples when $1-\lambda < (\omega_0\tau)^{4/3}$, i.e., in a small vicinity of the point $\lambda = 1$.

IV. RESONANT CASE

The resonant case is realized when ω_0 is large,

$$\omega_0\tau \gg 1. \quad (41)$$

The resonance takes place when $\omega \approx \omega_N$. For simplicity we will only consider the fundamental harmonics ($N=0$). Again, we search for the solution of Eqs. (4), (5), (7), and (8) in the following form:

$$U = U_0(x) + \frac{1}{2}U_1(x)e^{-i\omega t} + \frac{1}{2}U_1^*(x)e^{i\omega t} + \cdots, \quad (42)$$

$$v = v_d(x) + \frac{1}{2}v_1(x)e^{-i\omega t} + \frac{1}{2}v_1^*(x)e^{i\omega t} + \cdots, \quad (43)$$

where U_1 and v_1 are small compared to U_0 and v_d, respectively. Substituting Eqs. (42) and (43) into Eqs. (4), (5), (7), and (8) and averaging over time we get

$$\frac{\partial}{\partial x}\left(\frac{v_d^2}{2} + \frac{|v_1|^2}{4} + \frac{eU_0}{m}\right) + \frac{v_d}{\tau} = 0, \quad (44)$$

$$\frac{\partial}{\partial x}\left(U_0 v_d + \frac{U_1 v_1^* + U_1^* v_1}{4}\right) = 0. \quad (45)$$

The boundary conditions are

$$U_0(L)v_d(L) + \frac{U_1(L)v_1^*(L) + U_1^*(L)v_1(L)}{4} = \frac{j_d}{C}, \quad (46)$$

$$U_0(0) = U_g. \quad (47)$$

To solve these equations we should first find U_1 and v_1. One can see that the variations of U_0 and v_d are small,

$$\frac{U_0(0)-U_0(L)}{U_0(0)} \sim \frac{v_d(0)-v_d(L)}{v_d(0)} \sim \frac{v_d}{s}\frac{1}{\omega_0\tau} \ll 1. \quad (48)$$

Therefore, writing equations for U_1 and v_1 we can assume $U_0=\text{const}$, $v_d=\text{const}$, and

$$U_1, v_1 \sim e^{ikx}. \quad (49)$$

Linearizing Eqs. (4), (5), (7), and (8) we get

$$v_1\left(\frac{1}{\tau} - i\omega + ikv_d\right) + ik\frac{eU_1}{m} = 0, \quad (50)$$

$$U_1(-i\omega + ikv_d) + ikU_0 v_1 = 0, \quad (51)$$

$$U_1(0) = U_a, \quad U_1(L)v_d(L) + v_1(L)U_0(L) = 0. \quad (52)$$

For $s \gg v_d$ and $\omega\tau \gg 1$

$$k_\pm = \frac{\omega + i/2\tau}{s}\left(\pm 1 - \frac{v_d}{s}\right), \quad (53)$$

$$U_1 = C_+\frac{\omega - k_+ v_d}{k_+ U_0}e^{ik_+x} + C_-\frac{\omega - k_- v_d}{k_- U_0}e^{ik_-x}, \quad (54)$$

$$v_1 = C_+ e^{ik_+x} + C_- e^{ik_-x}. \quad (55)$$

Here

$$v_d = \frac{j_d}{CU_g}. \quad (56)$$

Using boundary conditions (52) we get

$$C_+ = \frac{U_a}{1 - \frac{k_-}{k_+}e^{i(k_+-k_-)L}}, \quad C_- = \frac{U_a}{1 - \frac{k_+}{k_-}e^{-i(k_+-k_-)L}}. \quad (57)$$

Equations (54)–(57) should be substituted into Eqs. (44) and (45). While solving Eq. (44), we will neglect the terms $v_d\partial v_d/\partial x$ and v_d/τ (one can show that this assumption is valid since $v_d/s \ll 1$ and $\omega_0\tau \gg 1$). Integrating Eq. (44) we have

$$U_0(L) - U_0(0) = \frac{1}{4}(|v_1(0)|^2 - |v_1(L)|^2). \quad (58)$$

Substituting Eqs. (53), (55), and (57) in Eq. (58) we have for detector response

$$\delta U_0(L) \approx \frac{U_a^2}{4U_g}\frac{\omega_0^2}{(\omega-\omega_0)^2 + \left(\frac{1}{2\tau} - \frac{v_d}{L}\right)^2}. \quad (59)$$

We see that response is a resonant function of the ω centered at $\omega = \omega_0$. The width of the resonant peak is given by

$$\frac{1}{2\tau_{eff}} = \frac{1}{2\tau} - \frac{v_d}{L}. \quad (60)$$

Since $v_d \sim j_d$, this width decreases with the current. For $v_d/L = 1/2\tau$, τ_{eff} turns to infinity. This condition coincides with the threshold condition for plasma wave generation.[3]

V. EXPERIMENT

The experiment was performed on a 250 nm gate length commercial GaAs HEMT (Fujitsu FHX06[35]) at room temperature using a 200 GHz Gunn diode as a radiation source. A waveguide ended with a metallic cone was connected to the output aperture of the Gunn diode to couple the radiation. The radiation power of the Gunn diode was approximately 20 mW. The sample was glued and wire-bounded on a quartz plate (in order to avoid the interference of THz radiation) and placed in an adjustable sample holder in front of the Gunn diode exit aperture. The radiation beam was not focused and the diameter of the "light spot" was approximately 10 mm at the position of the sample holder, i.e., much larger than the size of the device. No special coupling antennas were used in the experiment. The radiation most likely was coupled to the device through the metallization pads. The radiation intensity was modulated by the mechanical chopper at 140 Hz. The source terminal of the device was grounded. The dc drain current I_d was applied to the device and controlled by a Keithley Source Meter 2410. The source meter was operating in the current source mode, ensuring the asymmetry in the boundary conditions for the ac signal at the drain and source terminals. The dependence of the response, $\delta U_0(L)$, versus the drain current was measured using the standard lock-in technique at different gate biases. The gate bias was controlled by another Keithley source meter operated in the voltage source mode. The samples used in these studies were the same as were used in Ref. 26. Figures 1(a) and 1(b) show the current voltage characteristics of the GaAs HEMT under investigation. The essential device parameters such as the channel mobility, drain and source series resistances, channel length modulation parameter, etc. were determined first using the procedure described in Ref. 34. Then the characteristics in Fig. 1 were fitted using the above parameters as initial values for the Aim-Spice software.[36] The fitted curves (dashed lines in the figure) practically coincide with the measured characteristics. The fitting yielded the following transistor parameters: the source and drain series resistances $R_d = R_s = 4$ ohm, the field effect mobility, $\mu = 0.15\ \mathrm{m^2/V\,s}$, the effective electron saturation velocity $v_s = 2\times10^5$ m/s, ideality factor $\eta = 1.8$, and the device threshold voltage, $U_{th} = -0.38$ V. Figure 2 shows the nonresonant photoconductivity response of HEMT to the 200 GHz radiation, versus the drain current, I_d, at different values of the gate bias. V_{gs} varied from -0.35 V (which was slightly higher than the threshold voltage) up to -0.1 V. The response $\delta U_0(L)$ increased significantly with the drain current for a given gate bias, then saturated, reached a maximum, and then decreased. This maximum value of photo response monotonically decreased with increasing gate bias. Arrows in Fig. 2 show the values of current, corresponding to the velocity saturation. Solid curves in Fig. 2 are related to the theoretical calculations of the photoresponce using Eq. (A5). The theory developed in Sec. III does not account for the electron velocity saturation and it is applicable only to the linear region of operation of the transistor. Therefore, the theory can only be compared with the experimental data for I_d smaller than the current, corresponding to the velocity saturation. In the experiment, $\epsilon_0 = L^2\omega/\mu U_g$ varied in the range $3 \lesssim \epsilon_0 \lesssim 10$. Therefore, for discussion of the experi-

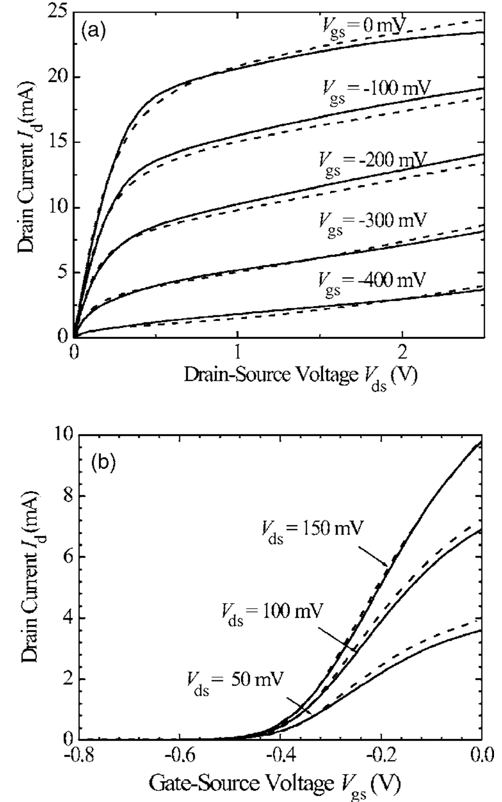

FIG. 1. $I_d - V_{ds}$ (a) and $I_d - V_{gs}$ (b) characteristics of GaAs HFET at different drain-source voltages (Ref. 26). Dashed curves correspond to theoretical calculations.

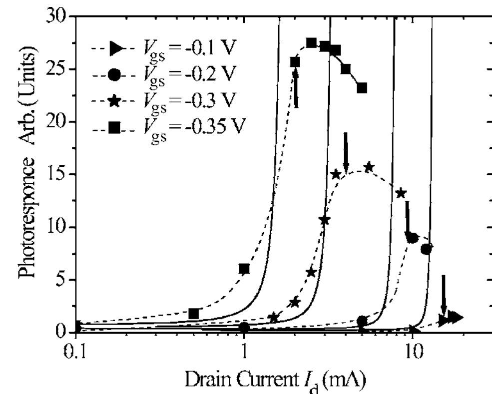

FIG. 2. Photoresponse of GaAs HEMT to 200 GHz radiation (characters), as a function of drain current at different gate biases. Dashed lines are drawn to guide an eye. Solid curves represent the theoretical dependencies. Arrows show the values of the current, corresponding to the velocity saturation.

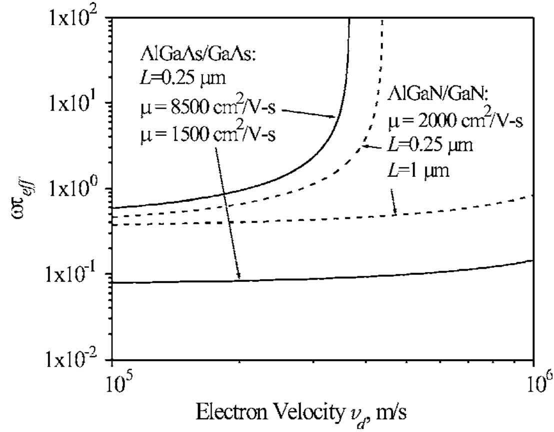

FIG. 3. Values of parameter $\omega\tau_{eff}$ calculated for different materials and different mobilities for $\omega = 200$ GHz.

mental results we should apply theory developed in Sec. III B. In derivation of Eq. (40), we used a gradual channel approximation [see Eq. (6)]. This approximation works well when the gate voltage is far from the threshold voltage ($e[V_{gs}-V_{th}] \gg T$, where T is the temperature). To achieve a better agreement with experiment, we generalized Eq. (40) in Appendix A to describe the gate voltage range close to V_{th} but still higher than V_{th} [see Eq. (A5)]. The response as a function of I_d is plotted on the Fig. 2 for different values of V_{gs}. We see that there is a reasonable agreement with the experiment.

The detailed experimental study of resonant case will be presented elsewhere.[26] Here we restrict ourselves by estimate of the factor $\omega\tau_{eff}$, which is responsible for the shape of the resonance curve. The values of $\omega\tau_{eff}$ are shown in Fig. 3 for different materials, different gate lengths and different mobilities. As seen, the values of $\omega\tau_{eff} > 1$ might be obtained at reasonable values of the electron drift velocities, allowing for the resonant detection by short channel FETs at room temperature.[26]

VI. DISCUSSION

In this section, we discuss the physical meaning of the obtained results. We start with discussing the nonresonant case. Above we have shown that a dc current dramatically increases the nonresonant detection amplitude both for short and long samples, especially when the drain voltage approaches the current saturation voltage. This voltage is related to an abrupt transition from the linear to saturation region of the current-voltage characteristic. Physically, the increase of the response is caused by increase of nonlinear properties of the FET channel, when the current flows in a FET and the concentration and field distributions become very nonuniform as illustrated in Fig. 4. Increasing the current and driving the transistor into saturation regime, the nonuniformity of the concentration and field distribution in the channel increases. Indeed, in the absence of radiation, theelectron concentration and potential at the drain $n_0(L), U_0(L)$ tend to zero, while the electric field at the drain

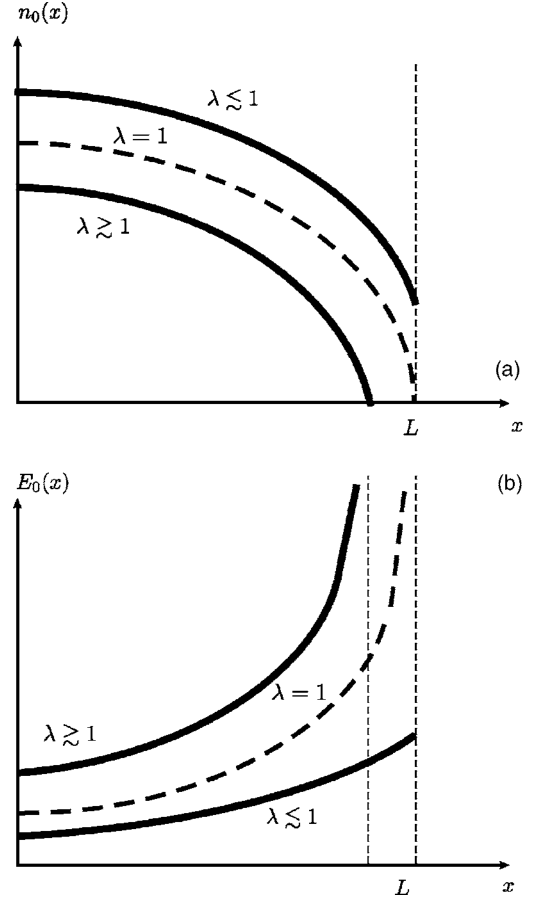

FIG. 4. Distributions of the averaged over time electron concentration (a) and dc component of electric field (b) along the channel of the transistor for $U_g^2 \approx 2j_dL/\mu C$ in the simplified constant mobility model. For the case $U_g^2 = 2j_dL/\mu C$ ($\lambda = 1$) these distributions are shown by dotted lines. This case corresponds to the pinch-off at the drain (i.e., to the drain saturation current). Notice the qualitative change when λ changes from the value less then unity to the value larger than unity. For $U_g^2 \gtrsim 2j_dL/\mu C$ ($\lambda \lesssim 1$), concentration and field at the drain $n_0(L), E_0(L)$ are finite, while in the case $U_g^2 \lesssim 2j_dL/\mu C$ ($\lambda \gtrsim 1$) concentration at the drain exactly equals to zero and electric field at the drain is infinite in the case of zero temperature. To get finite values of $n_0(L), E_0(L)$ at $\lambda > 1$, one has to take into account finite temperature effects.

$E_0(L) = -(\partial U_0/\partial x)_{x=L}$ tends to infinity when j_d tends to j_{sat} [see Eqs. (22), (24), and (25)] as follows:

$$n_0(L) = \frac{CU_g}{e}\sqrt{1-\lambda} \to 0, \qquad (61)$$

$$U_0(L) = U_g\sqrt{1-\lambda} \to 0, \qquad (62)$$

$$E_0(L) = -\left(\frac{\partial U_0}{\partial x}\right)_{x=L} = \frac{U_g}{2\sqrt{1-\lambda}}\frac{\lambda}{L} \to \infty, \qquad (63)$$

when $\lambda = j_d/j_{sat} \to 1$. We see that for the simplified constant mobility model used above, the electron concentration near the drain is zero in the saturation regime, while the electric field and, as a consequence, electron velocity are infinite

(this corresponds to "pinch-off" of the channel in the Shockley model). In reality, the velocity is limited by the effective saturation velocity, and the electric field and electron concentration remain finite but very large and small, respectively. Actually, the transition to the saturation regime takes place over the voltage range on the order of several thermal voltages, which is very small compared to the saturation drain voltage. Near the saturation voltage, even a small external field affects the small electron concentration and potential near the drain dramatically. This implies that the device becomes more sensitive to the external perturbations. To clarify this point, we use Eqs. (15) and (23), rewriting Eq. (62) as follows:

$$U_0(L) = \sqrt{U_g^2 - \frac{2j_dL}{\mu C}}. \tag{64}$$

This expression is nonanalytical at the saturation point $U_g^2 = 2j_dL/\mu C$ ($\lambda=1$). For $U_g^2 \gtrsim 2j_dL/\mu C$ ($\lambda \lesssim 1$), concentration $n_0(L), U_0(L)$ and $E_0(L)$ are finite, while in the case $U_g^2 \lesssim 2j_dL/\mu C$ ($\lambda \gtrsim 1$) $n_0(L)=0, U_0(L)=0$ and $E_0(L)=\infty$. The theoretically obtained distributions are plotted in Fig. 4 for $\lambda \approx 1$. It is clear from Fig. 4 that periodic variation of the gate voltage with arbitrary small amplitude leads to strong response at the saturation point: during one half of the period concentration and field at $x=L$ are finite while during the another part of the period concentration (field) at $x=L$ is equal to zero (infinity). In other words, response should be infinite at $\lambda=1$. This explains the physical origin of singularity in Eqs. (36) and (40). Actually, the response remains finite due to several reasons. First, we calculate response in the linear order with respect to U_a^2. One can show that this approximation is valid only when $U_a \ll U_g(1-\lambda)$ for $L \ll L_0$ and when $U_a \ll U_g\sqrt{1-\lambda}$ for $L \gg L_0$. Hence, response is limited by the value $\sim\sqrt{U_aU_g}$ for short samples and by the value $\sim U_a$ for long samples. Second, since $U_0(L)\to 0$, while $j_d \to j_{sat}$, the gradual channel approximation fails and one should use Eq. (A1) instead of Eq. (2). As we already mentioned, finite temperature effects smoothen transition to the saturation regime and lead to finite values of $n_0(L)$ and $E_0(L)$ in the saturation region. One can show that such effects limit the response by the value of the order of eU_a^2/T, where T is the temperature.

Let us now discuss the resonant case. In this case, the detection amplitude has maxima, when the radiation frequency is equal to fundamental plasma frequency and its harmonics [see Eq. (59)]. The resonant behavior is due to excitations of the plasma waves in the channel of the transistor by the electric field of the incident electromagnetic radiation.[3,9] We have shown that the resonant response might be strongly modified by so small current that the electron concentration in the channel is still homogeneous. Our main prediction is the decreasing of the effective resonant linewidth with the increasing current. As the velocity of the electron flow in the channel increases, the lower becomes the decrement of damping of plasma waves [see Eq. (60)]. This effective decrement, but not the electron-phonon or electron-impurity scattering, determines decay of the plasma oscillations in the channel of a FET. Physically, this decrease is due to approaching to the threshold of the plasma wave instability. Indeed, the second term in Eq. (60) responsible for decrease of damping is caused by the difference of the plasma wave velocity in the direction of the electron flow and opposite to the direction of the electron flow. This difference leads to the amplification of the plasma wave amplitude when reflected from the drain side of the channel.[3] As the velocity of the flow increased, the amplification leads to the plasma wave instability.[3] At some critical current value, corresponding to the condition $v_d=L/2\tau$, the width of the resonant response corresponding to the fundamental frequency would turn to zero, and the response at the fundamental frequency turns to infinity. This indicates the onset of plasma waves generation. In other words, the electric current shifts the system towards the threshold of the plasma wave instability predicted in Ref. 3. The extreme sensitivity of the detector in this current range is analogous to a sharp increase of sensitivity for different physical systems near the phase transition point.

VII. CONCLUSIONS

To conclude, we have considered the effect of the source-to-drain current on the terahertz detection by FET. In the nonresonant case, such a current sharply increases the detector response. In the resonant case, the current is predicted to decrease the resonance width. At a certain value of the current, this width should become zero. This value coincides with the threshold current for plasma waves generation. The theory of the nonresonant detection is in a reasonable agreement with experiment for positive values of the gate voltage swing.

ACKNOWLEDGMENTS

The work at RPI was supported by the STTR grant by ARO (subcontract from SET, Inc.) and CRDF (Project No. 2681). The research at Montpellier 2 University was supported by the French Ministry of Scientific Research, by the CNRS research group (GdR) "Solid State Detectors and Emitters of Terahertz Radiation." The work at Ioffe Physico-Technical Institute was supported by RFBR, a grant of the RAS, and a grant of the Russian Scientific School 2192.2003.2. The work of D. Veksler was supported by the NSF (Grant No. 0333314).

APPENDIX

Here we generalize Eq. (40) to take into account finite temperature effects. As a starting point we use the following expression for electron concentration in the channel[34]

$$n(x) = \frac{CT\eta}{e^2} \ln\left(1 + \exp\left[\frac{eU}{\eta T}\right]\right), \tag{A1}$$

where T is the temperature and $\eta \approx 2$ is the so-called ideality factor. Equation (6) is obtained from Eq. (A1) by taking a limit $T\to 0$).

The response should be calculated from the equation

$$\frac{\partial n}{\partial t} - \mu \frac{\partial^2 \chi}{\partial x^2} = 0, \tag{A2}$$

with the boundary conditions $j_d = -\mu \partial\chi/\partial x$ at $x=L$ and $U = U_g + U_a \cos \omega t$ at $x=0$. Here $\chi = \int_0^U n(U')dU'$. The calculations, quite analogous to ones presented in Sec. III B, yield

$$\delta U(L) = U_a^2 \alpha,$$

where coefficient α is expressed via properties of the stationary voltage-current curve

$$\alpha = \frac{[\partial n(U)/\partial U]|_{U=U_g}}{4n(U)|_{U=U_g - U^*}}. \tag{A3}$$

Here U^* is a voltage drop across the gated region for $U_a = 0$. Using Eq. (A1) we find

$$\left(\frac{\partial n(U)}{\partial U}\right)_{U=U_g} = \frac{C}{e} \frac{e^{eU_g/\eta T}}{1 + e^{eU_g/\eta T}}. \tag{A4}$$

As a result, we get the following expression for detector response:

$$\delta U(L) = \frac{eU_a^2}{4\eta T[1 + \exp(-eU_g/\eta T)]} \times \frac{1}{\ln\{1 + \exp[e(U_g - U^*)/\eta T]\}}. \tag{A5}$$

This equation reduces to Eq. (40) for $T \to 0$. Indeed, taking the limit $T \to 0$ in Eq. (A5) we get

$$\delta U(L) = \frac{U_a^2}{4(U_g - U^*)}. \tag{A6}$$

At $T=0$, the stationary I-V curve is given by Eq. (14), yielding

$$U^* = U_g - \sqrt{U_g^2 - \frac{2Lj_d}{\mu C}}.$$

Substituting U^* in Eq. (A6) we restore Eq. (40). For $T \neq 0$, the value of U^* can be extracted from experimental $I_d - V_{ds}$ curves [Fig. 1(a)] with account for the fact that U^* is not equal to measured voltage across sample V_{ds} because of finite voltage drop on the serial resistances of source and drain. The response as a function of I_d is plotted on the Fig. 2 for different values of V_{gs}.

[1] A. V. Chaplik, Zh. Eksp. Teor. Fiz. **62**, 746 (1972) [Sov. Phys. JETP **35**, 395 (1972)].

[2] M. S. Shur and L. F. Eastman, IEEE Trans. Electron Devices **26**, 1677 (1979).

[3] M. Dyakonov and M. Shur, Phys. Rev. Lett. **71**, 2465 (1993).

[4] A. P. Dmitriev, V. Yu. Kachorovskii, and M. S. Shur, Appl. Phys. Lett. **79**, 922 (2001).

[5] A. P. Dmitriev, A. S. Furman, and V. Yu. Kachorovskii, Phys. Rev. B **54**, 14020 (1996).

[6] A. P. Dmitriev, A. S. Furman, V. Yu. Kachorovskii, G. G. Samsonidze, and G. G. Samsonidze, Phys. Rev. B **55**, 10319 (1997).

[7] M. I. Dyakonov and M. S. Shur, Phys. Rev. B **51**, 14341 (1995).

[8] M. S. Shur and M. Dyakonov, Int. J. High Speed Electron. Syst. **9**, 65 (1998).

[9] M. Dyakonov and M. S. Shur, IEEE Trans. Electron Devices **43**, 380 (1996).

[10] S. J. Allen, Jr., D. C. Tsui, and R. A. Logan, Phys. Rev. Lett. **38**, 980 (1977).

[11] D. C. Tsui, E. Gornik, and R. A. Logan, Solid State Commun. **35**, 875 (1980).

[12] R. Weikle, J. Lu, M. S. Shur, and M. I. Dyakonov, Electron. Lett. **32**, 2148 (1996).

[13] J. Lu, M. S. Shur, J. L. Hesler, L. Sun, and R. Weikle, IEEE Electron Device Lett. **19**, 373 (1998).

[14] J. Lu, M. S. Shur, J. L. Hesler, L. Sun, and R. Weikle, *IEDM Technical Digest* (San Francisco, CA, 1998) pp. 879–882.

[15] P. J. Burke, I. B. Spielman, J. P. Eisenstein, L. N. Pfeiffer, and K. W. West, Appl. Phys. Lett. **76**, 745 (2000).

[16] W. Knap, V. Kachorovskii, Y. Deng, S. Rumyantsev, J. Q. Lu, R. Gaska, M. S. Shur, G. Simin, X. Hu, M. Asif Khan, C. A. Saylor, and L. C. Brunel, J. Appl. Phys. **91**, 9346 (2002).

[17] W. Knap, S. Rumyantsev, J. Lu, M. Shur, C. Saylor, and L. Brunel, Appl. Phys. Lett. **80**, 3433 (2002).

[18] W. Knap, Y. Deng, S. Rumyantsev, and M. S. Shur, Appl. Phys. Lett. **81**, 4637 (2002).

[19] W. Knap, F. Teppe, Y. Meziani, N. Dyakonova, J. Lusakowski, F. Buf, T. Skotnicki, D. Maude, S. Rumyantsev, and M. S. Shur, Appl. Phys. Lett. **85**, 675 (2004).

[20] W. Knap, Y. Deng, S. Rumyantsev, V. Kachorovskii, M. S. Shur, R. Gaska, G. Simin, and A. Khan, in *Proceedings of the Fourth International Conference on Nitride Semiconductors, Denver, Colorado, July 16–20, 2001*, edited by F. A. Ponce and A. Bell (Wiley-VCH 2002).

[21] X. G. Peralta, S. J. Allen, M. C. Wanke, N. E. Harff, J. A. Simmons, M. P. Lilly, J. L. Reno, P. J. Burke, and J. P. Eisenstein, Appl. Phys. Lett. **81**, 1627 (2002).

[22] X. G. Peralta, S. J. Allen, M. C. Wanke, J. A. Simmons, M. P. Lilly, J. L. Reno, P. J. Burke, and J. P. Eisenstein, in *Proceedings of the 26th International Conference on Physics of Semiconductors, Edinburgh, UK. 2002* (Institute of Physics, UK 2003).

[23] W. Knap, J. Lusakowski, T. Parenty, S. Bollaert, A. Cappy, V. Popov, and M. S. Shur, Appl. Phys. Lett. **84**, 2331 (2004).

[24] Y. Deng, R. Kersting, J. Xu, R. Ascazubi, Xi. Zhang, and M. S. Shur, Appl. Phys. Lett. **84**, 70 (2004).

[25] Taiichi Otsuji, Mitsuhiro Hanabe, and Osamu Ogawara, Appl. Phys. Lett. **85**, 2119 (2004).

[26] F. Teppe, D. Veksler, V. Yu. Kachorovskii, A. P. Dmitriev, S. Rumyantsev, W. Knap, and M. S. Shur, Appl. Phys. Lett. **87**, 052107 (2005).

[27] V. Dienys and J. Pozhela, *Hot Electrons* (Mintis, Vilnius, USSR, 1971).

[28] E. M. Conwell, *High Field Transport in Semiconductors* (Academic, New York, 1967).

[29] A. Satou, I. Khmyrova, V. Ryzhii, and M. S. Shur, Semicond. Sci.

Technol. **18**, 460, June (2003).
[30] V. Ryzhii, A. Satou, and M. S. Shur, Phys. Status Solidi A **202** R113 (2005).
[31] V. L. Kustov, V. I. Ryzhii, and Yu. S. Sigov, Sov. Phys. JETP **52**, 1207 (1980).
[32] V. Yu. Kachorovskii, I. S. Lioubinskii, and L. D. Tsendin, Phys. Rev. B **68**, 033308 (2003).
[33] Jian-Qiang Lü and M. S. Shur, Appl. Phys. Lett. **78**, 2587 (2001).
[34] T. Fjeldly, T. Ytterdal, and M. S. Shur, *Introduction to Device Modeling and Circuit Simulation* (John Wiley and Sons, New York, 1998); M. S. Shur, *Introduction to Electronic Devices* (John Wiley and Sons, New York, 1996).
[35] Fujitsu Microwave Semiconductor Databook (1999), Fujitsu Compound Semiconductor, Inc., 2355 Zanker Rd., San Jose, CA 95131-1138, USA.
[36] See http://www.aimspice.com/